Dynamic modeling framework for solid–gas sorption systems

Li, Dacheng; Lu, Tiejun; Hua, Nan; Wang, Yi; Zheng, Lifang; Jin, Yi; Ding, Yulong; Li, Yongliang

DOI:
10.1016/j.enss.2023.05.002

Document Version
Publisher's PDF, also known as Version of record

Citation for published version (Harvard):
Li, D, Lu, T, Hua, N, Wang, Y, Zheng, L, Jin, Y, Ding, Y & Li, Y 2023, 'Dynamic modeling framework for solid–gas sorption systems', *Energy Storage and Saving*, vol. 2, no. 3, pp. 522-531. https://doi.org/10.1016/j.enss.2023.05.002

Energy Storage and Saving 2 (2023) 522–531

Contents lists available at ScienceDirect

Energy Storage and Saving

journal homepage: http://www.keaipublishing.com/en/journals/energy-storage-and-saving/

Original article

Dynamic modeling framework for solid–gas sorption systems

Dacheng Li[a], Tiejun Lu[a], Nan Hua[a], Yi Wang[a], Lifang Zheng[b], Yi Jin[c], Yulong Ding[a], Yongliang Li[a,*]

[a] Birmingham Centre for Energy Storage, School of Chemical Engineering, University of Birmingham, Edgbaston, B15 2TT, United Kingdom
[b] School of Mechanical Engineering, University of Science and Technology Beijing, 100083, China
[c] Jiangsu Jinhe Energy Technology Co., Ltd, No.1, Sci & Tech Avenue, Economic and Technological Development Zone, Jiangsu Province, Jurong, China

ARTICLE INFO

Keywords:
Solid-gas sorption
Dynamic modeling
Intelligent optimization
Coefficient identification

ABSTRACT

A dynamic modeling framework based on an intelligent approach is proposed to identify the complex behaviors of solid-gas sorption systems. An experimental system was built and tested to assist in developing a model of the system performance during the adsorption and desorption processes. The variations in the thermal effects and gaseous environment accompanying the reactions were considered when designing the model. An optimization platform based on a multi-population genetic algorithm and artificial criteria was established to identify the modeling coefficients and quantify the effects of condition changes on the reactions. The calibration of the simulation results against the tested data showed good accuracy, where the coefficient of determination was greater than 0.988. The outcome of this study could provide a modeling basis for the optimization of solid-gas sorption systems and contribute a potential tool for uncovering key characteristics associated with materials and components.

1. Introduction

Reversible solid-gas sorption has been widely investigated and adopted in different energy applications such as refrigeration, heat pump, and energy storage systems [1–4]. Owing to the spontaneity of the reaction process, the application systems can be driven by low-grade waste heat or solar energy and can be integrated with working pairs with low global warming potential and zero ozone depletion potential [5,6]. Additionally, the high reaction enthalpy of solid-gas sorption compared with the sensible and latent heat leads to the capability of an efficient storage function to deal with the mismatches between the energy supply and demand and implement peak-shaving [7,8]. Therefore, the utilization of solid-gas sorption can greatly contribute to achieving decarbonization in energy sectors and reducing the economic expense of energy supply. However, the complex dynamic characteristics in the mass kinetics and heat transfer make the adsorption/desorption processes difficult to predict and therefore present obstacles to quantifying the parameters that influence the whole system performance [9]. Without fully clarifying the dynamic mechanism, it is difficult to optimize the system and extend its integration with intermittent renewables and fluctuating loads. This will lead to the reduction of the energy efficiency and increase the design and operation costs of sorption-based energy systems.

Two types of modeling are normally adopted to demonstrate the dynamic behavior of solid-gas sorption. A phenomenological model, which focuses on the detailed properties related to the specific reaction mechanism, has been studied and proposed [10–12]. A detailed understanding of the reaction phenomenon could be achieved using this type of model [13–15]. However, the inconveniences and difficulties in obtaining the parameters associated with the medium properties and system configurations make it difficult to develop a model with sufficient accuracy. Additionally, solving this kind of numerical model has a high computation cost, and the complexity of the model reduces its applicability to practical engineering problems. On the other hand, as reported in [16–18], the mass kinetics and heat transfer of the reaction can be considered in a global way. A detailed analysis of the elementary mechanisms is no longer needed in this approach. Instead, equivalent parameters are utilized to model the overall behavior of the phenomenon. Owing to the simplification of the modeling structure, a huge decrease in the computation cost compared to that of the phenomenological model can be expected. Therefore, a global model is preferred to describe the dynamic operation of a solid-gas sorption system, especially from the design and control points of view. In [17,18], the dynamic process of the reaction for a mixture of calcium chloride ($CaCl_2$) and methylamine (CH_3NH_2) was investigated using the global modeling approach. The medium transformation during two combined reactions and the heat

Peer review under responsibility of Xi'an Jiaotong University.
* Corresponding author.
E-mail address: y.li.1@bham.ac.uk (Y. Li).

https://doi.org/10.1016/j.enss.2023.05.002
Received 12 January 2023; Received in revised form 19 May 2023; Accepted 23 May 2023
Available online 26 May 2023

List of nomenclature

A	Heat transfer area, m^2
A_r	Arrhenius coefficient
C	Specific heat capacity, $kJ{\cdot}kg^{-1}{\cdot}K^{-1}$
c_1–c_9	Empirical parameters associated with enthalpy change
c_{10}–c_{14}	Empirical parameters associated with entropy change
E	Activation energy, $kJ{\cdot}mol^{-1}$
F	Punishment element
h	Heat transfer coefficient, $kW{\cdot}m^{-2}{\cdot}K^{-1}$
i	ith time segment
j_1–j_4	Coefficients of equivalent gas transfer between the buffer tank and reactor
k_1–k_4	Coefficients of equivalent gas transfer between the adsorption phase and gaseous phase
m	Mass, kg
M	Kinetic coefficient related to modeling of adsorption
n	Number of moles
N	Kinetic coefficient related to modeling of desorption
NS	Total number of time segments
P	Pressure, bar
Q	Heat, kJ
R	Universal gas constant, $J{\cdot}mol^{-1}{\cdot}K^{-1}$
t	Time
T	Temperature, K
U	Uncertainty
V	Volume, m^3
w	Uptake mass, kg
W	Weighting coefficient
X	Global advancement
Xr	Reaction rate

Greek symbols

γ	Specific heat ratio of adsorbate
ΔH	Change in enthalpy, $kJ{\cdot}mol^{-1}$
ΔS	Change in entropy, $kJ{\cdot}K^{-1}{\cdot}mol^{-1}$
ρ	Density, $kg{\cdot}m^{-3}$

Subscripts

ad	Adsorption
bt	Buffer tank
bte	Equivalent influence of buffer tank
de	Desorption
g	Gas
gp	Gaseous phase
eq	Equilibrium
et	Equivalent
ms	Measured
pe	Equivalent transfer between gaseous and adsorption phases
re	Reactor
s	Solid adsorbent
sm	Simulation

Abbreviation

HTF	Heat transfer fluid
MGA	Multi-population genetic algorithm
SEM	Scanning electron microscopy

transfer across the reacting bed were modeled. Huang et al. [19] selected a global modeling structure to describe the global advancement and temperature of a fixed-bed reactor that used $SrCl_2$ as the solid adsorbent and NH_3 as the gas adsorbate. A sensitivity analysis of the simulation results was also conducted to determine the influences of the thermal parameters on the reactor performances. Nagamalleswara et al. [20] investigated the thermodynamic properties of $BaCl_2$ and expanded natural graphite composites compared with those of pure $BaCl_2$. The kinetic coefficients for the adsorption and desorption with ammonia adsorbate were quantified using global reaction rate modeling. Bao et al. [21] developed a whole system model for a cogeneration unit integrated with chemisorption refrigeration. A global model for a refrigeration system that used $MnCl_2$ and NH_3 as the working pairs was established. This model was then combined with the dynamic modeling of an expander to demonstrate the overall viability of the cogeneration performance. Despite acceptable agreement between the simulation results and tested data achieved in these studies, restrictions still exist when using the current modeling structure to clarify the dynamic behavior of a sorption-based system. The current modeling mainly focuses on the dynamic performance of the system under an isobaric condition in the reactor. The variation of the gas mass in the reactor accompanying both the adsorption and desorption processes in a real application context has not been considered, and no study has been conducted to illustrate how a change in the gaseous environment would influence the system performance. Moreover, an intelligent platform that can efficiently identify the modeling coefficients by tracking the effects of nonlinear dynamics has not been proposed.

In this study, a dynamic modeling framework was established to investigate the behaviors of solid-gas sorption systems. An experimental system was built using activated carbon and carbon dioxide as the working pair. Owing to the low cost, good sorption performance, and great reversibility, this working pair has been widely explored from the perspectives of adsorbent components and structures [22–24]. Tests were conducted to analyze the factors that influenced the dynamic performance of solid-gas sorption and to provide real-time operation data for the subsequent validation of the modeling and framework. A semi-empirical global model of the adsorption and desorption processes was developed considering the mass change in the gaseous adsorbate accompanying the reactions in a closed system. Then, an intelligent optimization platform based on a multi-population genetic algorithm (MGA) and artificial criteria was developed to identify the modeling coefficients and predict unrevealed parameters. After a discussion of the simulation results, the conclusions of this study are provided. Additionally, suggestions are given for further improving the modeling and platform and for future studies to optimize the design and control of a solid-gas sorption system.

2. Experimental setup and analysis

2.1. Experimental apparatus

As shown in Fig. 1, an experimental solid-gas sorption system was constructed. The system mainly consisted of a cylindrical fixed-bed reactor 1 with a jacket, a buffer tank 2, a thermostat 3, and valves 4–7. Activated carbon (Norit® R 2030 CO2, CABOT Corporation USA) was adopted as the solid adsorbent and used to fill the reactor. The scanning electron microscopy (SEM) image of Fig. 2 shows many porous structures on the surface of the activated carbon, which was beneficial for the adsorption of the gas phase molecules. Two thermocouples, T_1 and T_2, were mounted inside the top and bottom parts of the reactor, and the average value was used to represent the temperature of the reactor. Carbon dioxide (BOC, UK) from a high-pressure vessel was used as the gas adsorbate and stored in the buffer tank, where the temperature was measured by thermocouple T_3. Two pressure gauges, P_1 and P_2, were installed and utilized to measure the pressure variation in the reactor and buffer tank, respectively. To maintain the required environment temperature of the reactor, water at a temperature controlled by the thermostat was adopted as the heat transfer fluid (HTF) and circulated through the outer jacket of the reactor. The design parameters of the test rig are given in Table 1.

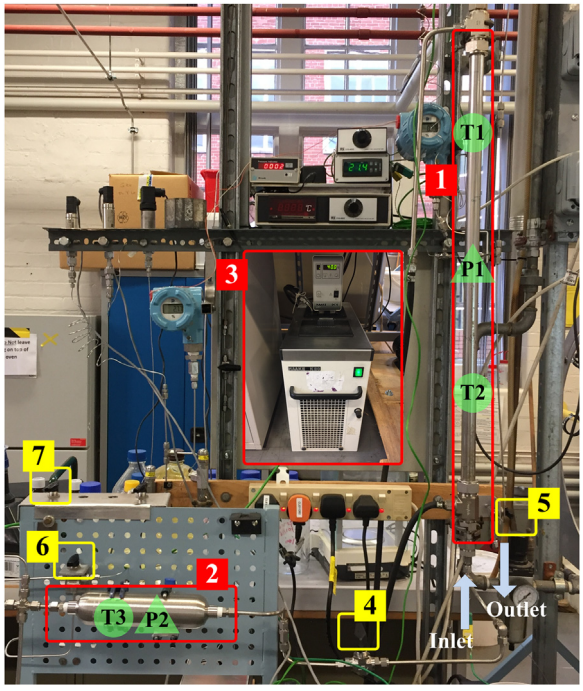

Fig. 1. Experimental solid-gas sorption system.

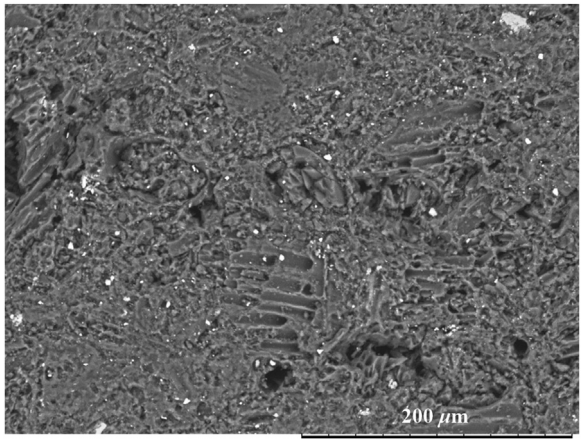

Fig. 2. Scanning electron microscopy (SEM) image of the activated carbon sample.

2.2. System operation and test results

2.2.1. Thermal effect analysis

In physical solid-gas sorption, which was adopted in this study, the changes in the enthalpy and entropy vary with the global advancement of the reaction [25]. This phenomenon is mainly attributed to the inhomogeneities of the surface energy distribution of the solid adsorbent and, in turn, affects the degree of the reaction. During the adsorption process, gas molecules will first be adsorbed on surfaces with lower activation energy. Then, with an increase in the surface coverage, the gas will gradually be adsorbed by the less activated adsorption sites. The transport of the gas phase will proceed in a reverse direction when the desorption process occurs. To investigate the changes in the thermal effects with gas uptake and provide essential parameters for the modeling design, equilibrium tests were conducted by regulating the amount of gas input into the reactor. The test procedure is illustrated below, with references to the flowchart of Fig. 1.

Table 1
Design parameters of the test rig.

Parameter	Value
Volume of the reactor ($\times10^{-3}$, m^3)	0.23
Inner diameter of the reactor ($\times10^{-3}$, m)	15.85
Effective length of the reactor (m)	0.80
Mass of activated carbon ($\times10^{-3}$, kg)	65.60
Density of activated carbon ($\times10^{3}$, $kg{\cdot}m^{-3}$)	2.20
Volume of the buffer tank ($\times10^{-3}$, m^3)	0.33
Pressure of the CO_2 vessel (bar)	53
Thermostat temperature range (K)	278.15–368.15
Range and accuracy of thermocouple (K, K)	233.15–1373.15, ±1.50
Range and accuracy of pressure gage (bar, %)	0–40, ±0.25

Step 1: Valve 4 is closed and valve 5 is opened. The reactor is heated to 313.15 K by the circulating water via the outer jacket, and full gas desorption is conducted under normal atmospheric pressure (101,325 Pa).

Step 2: Valves 6 and 7 are opened. The buffer tank is charged to the required initial pressure using the CO_2 from the high-pressure vessel, and then valves 6 and 7 are closed.

Step 3: Valve 5 is closed. The reactor is cooled to 293.15 K by the circulation water and reaches an initial equilibrium state, $S0$.

Step 4: Valve 4 is opened. The gas stored in the buffer tank enters the reactor, and the reaction reaches a new equilibrium state, $S1$.

Step 5: Valve 4 is closed, and the gas mass inside the reactor is fixed. Then, the reactor is heated from 293.15 K to 308.15 K in 5 °C steps, and new equilibrium states are obtained: $S2$, $S3$, and $S4$.

Steps 1 to 5 are repeated for different gas mass inputs (by regulating the initial pressure of the buffer tank in Step 2). According to the Clausius-Clapeyron relationship shown below, the changes in the enthalpy (ΔH) and entropy (ΔS) can be determined using the system conditions under equilibrium states $S1$ to $S4$:

$$P_{eq} = \exp\left(\frac{\Delta H}{RT_{re}} + \frac{\Delta S}{R}\right) \tag{1}$$

where P_{eq} and T_{re} refer to the equilibrium pressure and temperature of the reactor, respectively; and R refers to the universal gas constant. The variation of the temperature and pressure of the reactor could be measured directly using the sensors, while the total gas mass input to the reactor at time t was calculated based on the change in the density of the gas in the buffer tank compared with that at the initial moment, 0, as follows:

$$m_g(t) = \left(\rho_g\left(T_{bt}, P_{bt}\right)|_0 - \rho_g\left(T_{bt}, P_{bt}\right)|_t\right)V_{bt} \tag{2}$$

where ρ_g refers to the gas density; T_{bt} and P_{bt} refer to the temperature and pressure of the buffer tank, respectively; and V_{bt} refers to the volume of the buffer tank.

Then, the accumulated gas uptake, w_{ad}, at time t can be calculated as follows:

$$w_{ad}(t) = m_g(t) - (\rho_g(T_{re}, P_{re})|_t - \rho_g(T_{re}, P_{re})|_0)(V_{re} - V_s) \tag{3}$$

where V_{re} and V_s refer to the volumes of the reactor and solid adsorbent, respectively; and P_{re} refers to the pressure of the reactor.

The factors that affected the test results included the uncertainties in the measurements of the reactor temperature (U_1), buffer tank temperature (U_2), reactor pressure (U_3), and buffer tank pressure (U_4). The standard uncertainties related to these measurements were obtained based on a verification report for the sensors and are listed in Table 2.

Table 2
Standard uncertainties of measurements.

U_1 (K)	U_2 (K)	U_3 (%)	U_4 (%)
0.87	0.87	0.14	0.14

Table 3
Enthalpy and entropy changes of the reaction under various gas inputs.

Initial gage pressure of buffer tank (bar)	Gas input (g)	Gas uptake (g)	ΔH (kJ·mol^{-1})	ΔS (J·K^{-1}·mol^{-1})
40	19.86	11.39	−8.39	149.32
30	15.08	9.72	−11.00	154.70
20	10.87	8.45	−15.38	163.33
10	5.86	4.54	−19.80	171.20
6	3.42	2.93	−21.31	172.05
4	2.37	2.03	−19.24	163.37
2	1.32	1.14	−20.24	164.00
1	0.78	0.61	−18.42	157.42

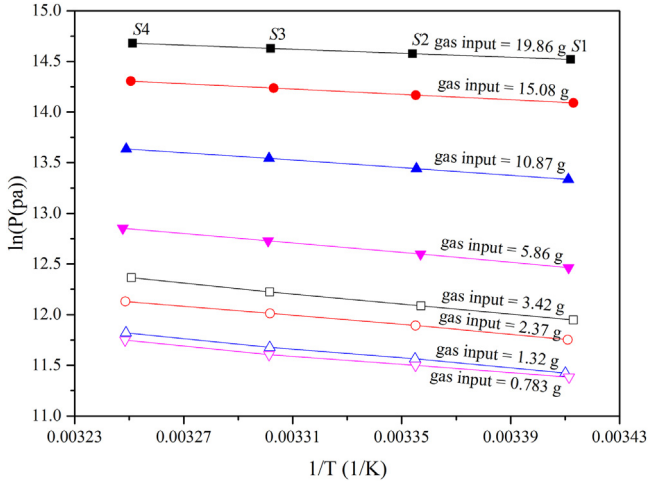

Fig. 3. Equilibrium reaction lines under different gas mass inputs.

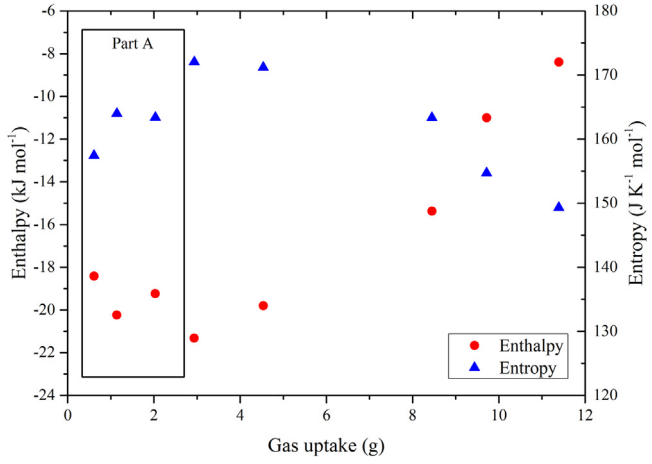

Fig. 4. Enthalpy and entropy changes under different gas mass uptakes.

Referring to Table 3, eight sets of experiments under conditions with different gas mass inputs were conducted, and the results are depicted in Figs. 3 and 4. Differences in the slope and intercept between equilibrium lines verified the unevenness of the active surface of the adsorbent. It is worth noting that the thermal effect did not always vary monotonically with an increase in the gas input. Referring to Part A in Fig. 4, fluctuations in the reaction enthalpy and entropy changes can be observed under the condition of a relatively low gas input (< 3.42 g). One possible reason for this phenomenon is the filling structure of the activated carbon particles, which created gas passages inside the reactor. Specifically, gas entered from the bottom of the reactor and travelled through these passages. The gas was absorbed by nearby active surfaces with less traveling resistance, even though more energy was required for the adsorption. If an equilibrium state was achieved at this point, smaller changes in the enthalpy and entropy of the reaction were observed. With an increase in the gas input, sufficient driving forces could be provided for the gas molecules to travel further and react with the higher-activity surfaces. This resulted in greater changes in the enthalpy and entropy and led to fluctuations in the thermal effects at the equilibrium state. As the low-traveling-resistance surfaces became occupied by more input gas, the reaction proceeded sequentially with high-activity and low-activity surfaces, causing the thermal effect to vary in a monotonic manner.

To describe the thermal effects under different amounts of gas input and gas uptake, a quartic polynomial relationship and dose-response relationship were adopted, respectively, to model the monotonically varying part (gas input ≥ 3.42 g) shown in Fig. 3, which can be represented as follows:

$$\begin{cases} \Delta H(m_g) = c_1 m_g^4 + c_2 m_g^3 + c_3 m_g^2 + c_4 m_g + c_5 \\ \Delta S(m_g) = c_{10} m_g^4 + c_{11} m_g^3 + c_{12} m_g^2 + c_{13} m_g + c_{14} \end{cases} \tag{4}$$

$$\Delta H(w_{ad}) = c_6 + (c_7 - c_6)/\left(1 + 10^{(c_8 - w_{ad})\times c_9}\right) \tag{5}$$

where empirical parameters c_1 to c_{14} can be obtained by curve fitting against the tested data. The fluctuations in the enthalpy and entropy changes at low gas inputs (< 3.42 g) will be discussed in our future work.

2.2.2. Dynamic performance

The dynamic behavior of the system under a changing gaseous environment was investigated by conducting Step 4 described in Section 2.2.1. The global advancement of the reaction at time t could be evaluated as follows:

$$X(t) = \frac{w_{ad}(t)}{w_{ad}(t_{eq})} \tag{6}$$

Then, the reaction rate at time t could be determined as follows:

$$Xr(t) = X_{ad}(t) - X_{ad}(t-1) \tag{7}$$

Three sets of experiments were conducted to investigate the dynamic performance of the reaction under a monotonical variation of the thermal effects. The initial pressure of the buffer tank was set at 40 bar, 20 bar, and 6 bar, and the corresponding tested data and evaluated results are presented in Figs. 5–7, respectively.

For the 40 bar case, as shown in Fig. 5, sharp increases in the pressure and uptake rate can be observed at the beginning stage of the adsorption (Section 1) owing to the continuous gas input from the buffer tank. With the rise of global advancement, thermal energy was released from the reaction and resulted in an increase in the temperature in the reactor (Section 2). The elevated temperature, reduction of the high-activity reaction area, and decrease in the gas input rate had negative effects on the adsorption. Therefore, a drop in the uptake rate can be observed in Section 3 as the reaction proceeds. It is worth noting that a negative uptake rate even occurred, and the desorption process was carried out (Section 4). Some of the adsorbed CO_2 was released from the adsorbent, and global advancement went down (Section 4). A portion of the CO_2

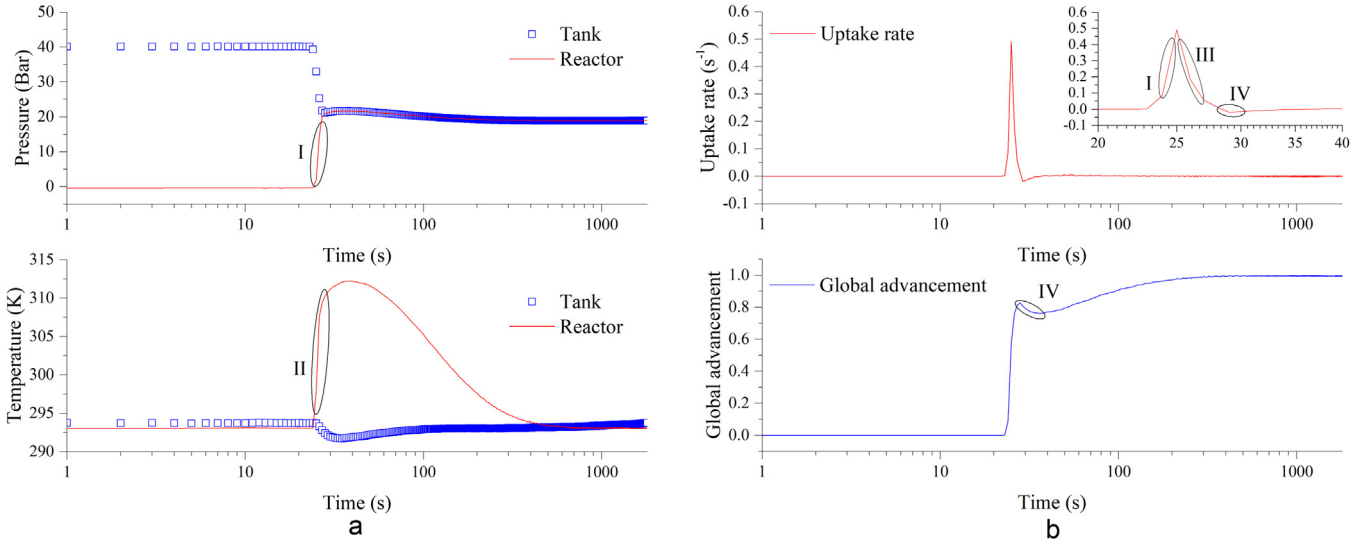

Fig. 5. Dynamic behavior of the reaction process (initial buffer tank pressure = 40 bar). (a) Pressure and temperature; (b) uptake rate and global advancement.

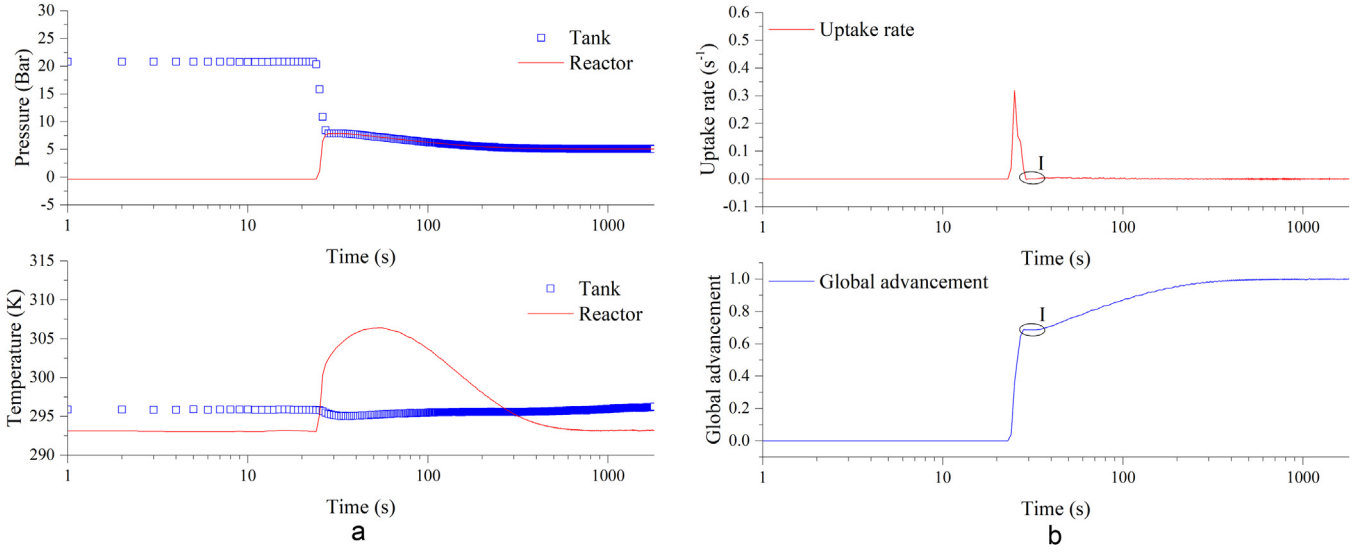

Fig. 6. Dynamic behavior of the reaction process (initial buffer tank pressure = 20 bar). (a) Pressure and temperature; (b) uptake rate and global advancement.

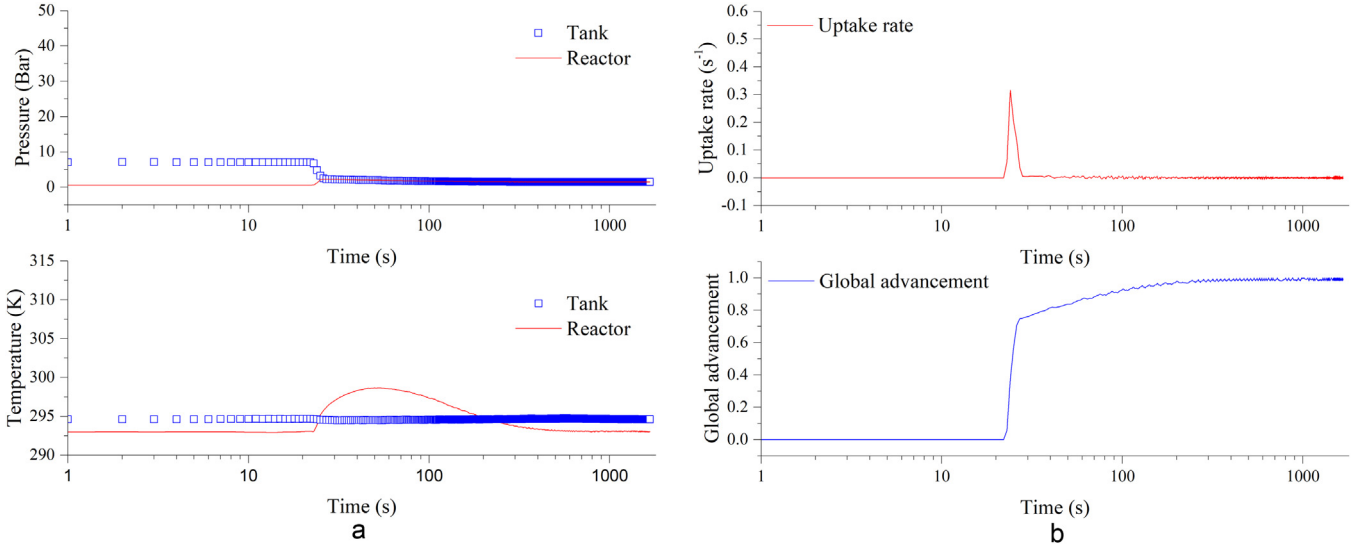

Fig. 7. Dynamic behavior of the reaction process (initial buffer tank pressure = 6 bar). (a) Pressure and temperature; (b) uptake rate and global advancement.

even refluxed to the buffer tank and contributed to extending the desorption process. In the subsequent stage, a pressure rise caused by the continuous gas release, heat absorbed by the desorption and HTF, and regain of the high-activity areas altered the reaction, resulting in the occurrence of the adsorption process again. Similar dynamic characteristics could be observed when the initial pressure of the buffer tank was set to 20 bar (Fig. 6), where the intensity of the reaction was weakened, and the duration of the alternating desorption process was shortened (Section 1). Referring to Fig. 7, a monotonical increase in global advancement can be seen when the initial pressure of the buffer tank was reduced to 6 bar. The uptake rate maintained a positive value during the whole process. The alternating desorption did not emerge because the negative influence that occurred along with the adsorption process was not strong enough to change the trend of the reaction.

Based on the experimental results presented above, the system experienced complicated reaction processes in a changing gaseous environment. The reaction was not only coupled with the kinetics of the mass and heat transfer inside the reactor, but it was also influenced by the dynamic gas mass and heat transfer with the external environment.

3. Dynamic modeling of solid-gas sorption

The dynamic model of the solid-gas sorption process was developed based on the aspects of both the mass and heat transfer inside the reactor considering the variation of the gaseous environment. To facilitate the modeling work, the following assumptions were made considering practical engineering applications.

At a certain moment,

(i) the temperature and pressure gradients in the radial and axial directions inside the reactor are ignored, and a uniform temperature and pressure throughout the reactor are assumed;
(ii) a high flow rate for the heat transfer fluid is imposed on the outer jacket of the reactor, and the reactor is located in a uniform temperature environment;
(iii) identical temperatures are assumed for the gas and solid in the reactor, and this temperature is adopted to represent the overall temperature of the reactor.

3.1. Global advancement modeling

The rate of global advancement, which represents the mass transfer with regard to the evolution of the reaction, is generally described as follows [17,26]:

$$\frac{dX(t)}{dt} = f(X)\cdot K\left(P_{re}, T_{re}\right) \tag{8}$$

where $f(X)$ represents the influence of the current state of advancement on the reaction rate, and $K(P_{re},T_{re})$ describes the dependency of the reaction rate on the pressure and temperature deviations of the reactor from the equilibrium conditions [17].

The expression $[1-X(t)]^{M(N)}$ is normally adopted for $f(X)$ to describe the effect of a change in the reacting surface area on the sorption [27], where M and N refer to the kinetic coefficients related to the modeling of the adsorption and desorption, respectively. On the other hand, the following equations have been developed to represent $K(P_{re},T_{re})$ considering Arrhenius' law for solid-gas sorption [16]:

$$K\left(P_{re}, T_{re}\right) = \begin{cases} Ar_{ad}\cdot exp\left(-\frac{E_{ad}}{RT_{re}}\right)\cdot\left(\frac{P_{re}-P_{eq}(m_g,T_{re})}{P_{re}}\right) \\ Ar_{de}\cdot exp\left(-\frac{E_{de}}{RT_{re}}\right)\cdot\left(\frac{P_{eq}(m_g,T_{re})-P_{re}}{P_{eq}(m_g,T_{re})}\right) \end{cases} \tag{9}$$

where Ar and E represent the Arrhenius coefficient and activation energy, respectively.

As discussed in Section 2.2.2, during the reaction, a gas transfer between the buffer tank and reactor is induced by a differential pressure. The movement of gas molecules between the adsorption and gas phases is driven by deviations from the equilibrium condition. These processes continuously and simultaneously affect the progress of the reaction. To integrate these dynamic elements into the modeling design, in this study, an equivalent adsorbate mass that represented the average gas mass participating in the reaction in a certain period of time was proposed and defined as follows:

$$m_{et}(t) = m_{bte}(t) + m_{pe}(t) + m_g(t-1) \tag{10}$$

The equivalent gas transfer between the buffer tank and reactor, m_{bte}, is represented using a linear relationship:

$$m_{bte}(t) = \begin{cases} j_1\left(P_{re}(t-1) - P_{bte}(t-1)\right) + j_2;\ if\ P_{re}(t-1) > P_{bte}(t-1) \\ j_3\left(P_{bte}(t-1) - P_{re}(t-1)\right) + j_4;\ if\ P_{re}(t-1) \le P_{bte}(t-1) \end{cases} \tag{11}$$

In Eq. (11), the equivalent pressure of the buffer tank under temperature T_{re} is found as follows:

$$P_{bte} = P_{bt}\left(\frac{T_{bt}}{T_{re}}\right)^{\frac{\gamma}{1-\gamma}} \tag{12}$$

where γ refers to the specific heat ratio of the adsorbate.

On the other hand, the equivalent gas transfer between the adsorption phase and gaseous phase, m_{pe}, is shown in the following form:

$$m_{pe}(t) = \begin{cases} k_1\left(P_{re}(t-1) - P_{eq}(t-1)\right) + k_2;\ if\ P_{re}(t-1) > P_{eq}(t-1) \\ k_3\left(P_{eq}(t-1) - P_{re}(t-1)\right) + k_4;\ if\ P_{re}(t-1) \le P_{eq}(t-1) \end{cases} \tag{13}$$

In Eqs. (11) and (13), coefficients j_1 to j_4 and k_1 to k_4 need to be identified by calibrating the model using experimental results.

The duration of the system operation is divided into multiple equal time segments. For each time segment, the equilibrium pressure represented by Eq. (1) is calculated using the equivalent adsorbate mass obtained by Eq. (10). On the other hand, the equivalent pressure in the reactor under m_{et} is evaluated using the following equation:

$$P_{et} = \frac{\left(m_{et}(t) - w_{ad}\left(t_{eq}\right)X(t-1)\right)RT_{re}(t-1)}{\left(V_{re} - V_s\right)} \tag{14}$$

P_{eq} and P_{et} are compared in each time segment to determine the trend of the reaction.

3.2. Temperature modeling

In the adsorption process, the heat released from the reaction is diffused into the HTF and absorbed by the adsorbent and adsorbate in the reactor. During the desorption process, the heat input from the HTF is absorbed by the reaction and transferred to the adsorbate and adsorbent. Based on the thermal balance, the dynamic variation of the reactor temperature can be modeled as follows:

For adsorption,

$$\begin{aligned}&\left(C_s m_s + C_{gp}m_{gp}(t) + C_{ad}w_{ad}(t)\right)\frac{dT_{re}(t)}{dt} + C_{gp}\Delta m_g(t)\left(T_{re}(t-1) - T_{bt}(t-1)\right) \\ &= Q(t) - hA\left(T_{re}(t-1) - T_{HTF}(t-1)\right)\end{aligned} \tag{15}$$

where

$$\begin{cases} \Delta m_g(t) = m_g(t) - m_g(t-1) \\ Q(t) = -\left(w_{ad}(t) - w_{ad}(t-1)\right)\left(\Delta H(t) + \Delta H(t-1)\right)/2/n_g \end{cases} \tag{16}$$

and for desorption,

$$\left(C_s m_s + C_{gp}m_{gp}(t) + C_{ad}w_{ad}(t)\right)\frac{dT_{re}(t)}{dt} = Q(t) + hA\left(T_{HTF}(t-1) - T_{re}(t-1)\right) \tag{17}$$

In Eqs. (15) to (17), C_s, C_{gp}, and C_{ad} refer to the specific heat capacities of the solid adsorbent, and the adsorbate in the form of the gas and adsorption phases, respectively; m_s and m_{gp} refer to the masses of the

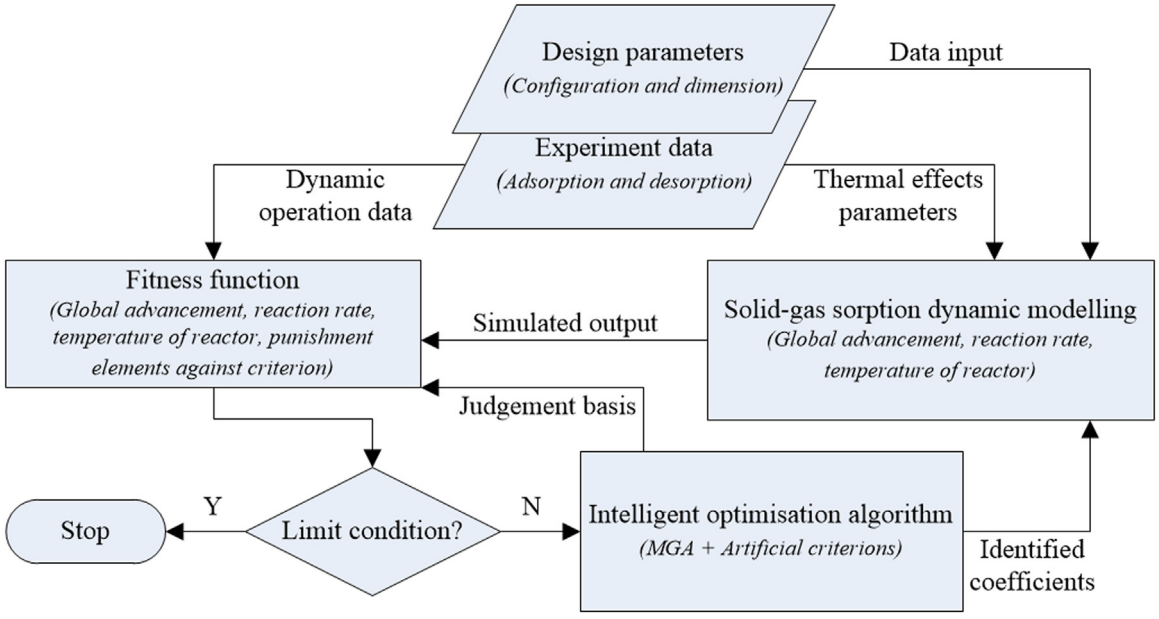

Fig. 8. Optimal identification framework.

adsorbent and gas-phase adsorbate in the reactor, respectively; Q refers to the heat of the reaction; h and A refer to the heat transfer coefficient and heat transfer area between the reactor and HTF, respectively; T_{HTF} refers to the temperature of the heat transfer fluid; and n_g refers to the number of moles of adsorbate.

4. Optimization framework

To identify the dynamic characteristics of the solid-gas sorption process, as shown in Fig. 8, an intelligent optimization framework based on an MGA was established. Compared to a standard genetic algorithm, an MGA involves multiple populations that can use different evolution parameters. This can help avoid premature convergence and enhance the ability to search for optimal solutions [28,29]. Potential combinations of modeling coefficients are evolved and produced with the generation according to their fitness degree and using natural genetics. On the other hand, artificial criteria were designed and incorporated into the framework to monitor the alternating gas uptake and release during the reaction, while also ensuring that the equivalent mass remained within a reasonable value range.

The fitness function of the framework was composed of three parts. Referring to Eqs. (18)–(21), Part I was formed by the sum of punishment elements, F_1, which were produced by the inconsistent direction of the gas transfer between the gas and adsorption phases obtained from the simulation and direct measurement; Part II was the sum of punishment elements, F_2, which arose when the simulated equivalent gas mass exceeded a reasonable range; and Part III was defined using the sum of the absolute values of the errors between the measured operating data and simulated results.

$$Fitness = \text{Fitness}|_{\text{I}} + \text{Fitness}|_{\text{II}} + \text{Fitness}|_{\text{III}} \tag{18}$$

$$\text{Fitness}|_{\text{I}} = \sum_{i=1}^{\text{NS}} \left(\text{F}_1(\text{i})\right) \tag{19}$$

$$\text{Fitness}|_{\text{II}} = \sum_{i=1}^{\text{NS}} \left(\text{F}_2(\text{i})\right) \tag{20}$$

$$\text{Fitness}|_{\text{III}} = \frac{1}{\text{NS}} \sum_{i=1}^{\text{NS}} \left(W_X \frac{|X_{\text{sm}}(\text{i}) - X_{\text{ms}}(i)|}{\max(X_{\text{ms}}(i))} + W_{\text{Xr}} \frac{|Xr_{\text{sm}}(i) - Xr_{\text{ms}}(i)|}{\max(Xr_{\text{ms}}(i))} + W_T \frac{|T_{\text{sm}}(i) - T_{\text{ms}}(i)|}{\max(T_{\text{ms}}(i))} \right) \tag{21}$$

where NS refers to the total number of time segments, i; X_{sm}, Xr_{sm}, and T_{sm} refer to the simulated global advancement, reaction rate, and temperature of the reactor, respectively; and X_{ms}, Xr_{ms}, and T_{ms} refer to the corresponding measured data. W_X, W_{Xr}, and W_T refer to the weighting coefficients of the global advancement, reaction rate, and temperature of the reactor, respectively.

The logical procedure of the criteria flowchart shown in Fig. 9 is conducted in each time segment. In Loop A, a positive measured reaction rate reveals that the system is undergoing an adsorption process. In this context, the equilibrium pressure calculated using m_{et} should be lower than the equivalent pressure calculated by Eq. (14). In contrast, if a negative reaction rate is measured, a desorption process proceeds, and the equilibrium pressure is higher than the equivalent pressure in the reactor. The inconsistency of the gas uptake or release judged by the measured reaction rate and a comparison of P_{eq} and P_{et} will activate F_1. In Loop B, the gas mass in the buffer tank (m_{bt}) and mass of the gas phase (m_{gp}) and adsorption phase (w_{ad}) in the reactor are combined to impose reasonable limitations for m_{et} in segment i. Any simulated m_{et} beyond these ranges will be deemed as irrational, and punishment value F_2 will be added to the fitness function.

5. Results and discussion

To identify the coefficients associated with the dynamic modeling, the measured data and simulation results were compared in relation to the global advancement, reaction rate, and temperature of the reactor. The empirical parameters related to the monotonical variation of the thermal effects were obtained first. The data provided in Table 3 were used to fit Eqs. (4) and (5), and the results are given in Table 4. In the current study, the dynamic behavior of the test system in the 40 bar case was adopted and evaluated to conduct the calibration work. The alternating gas uptake and release in this case (shown in Fig. 5) could assist in the simultaneous identification of the adsorption and desorption performances using one set of operation data. To increase the accuracy of the calibration, the coefficients related to the mass transport and heat transfer were separately identified using the designed optimization framework shown in Fig. 8. The main parameters related to the MGA were set as follows: the dimensions of the variables were 14 and 2 for the global advancement modeling and temperature modeling, respectively; the population number was 10; and the individual number in each population was 20. The densities of the gas in the buffer tank

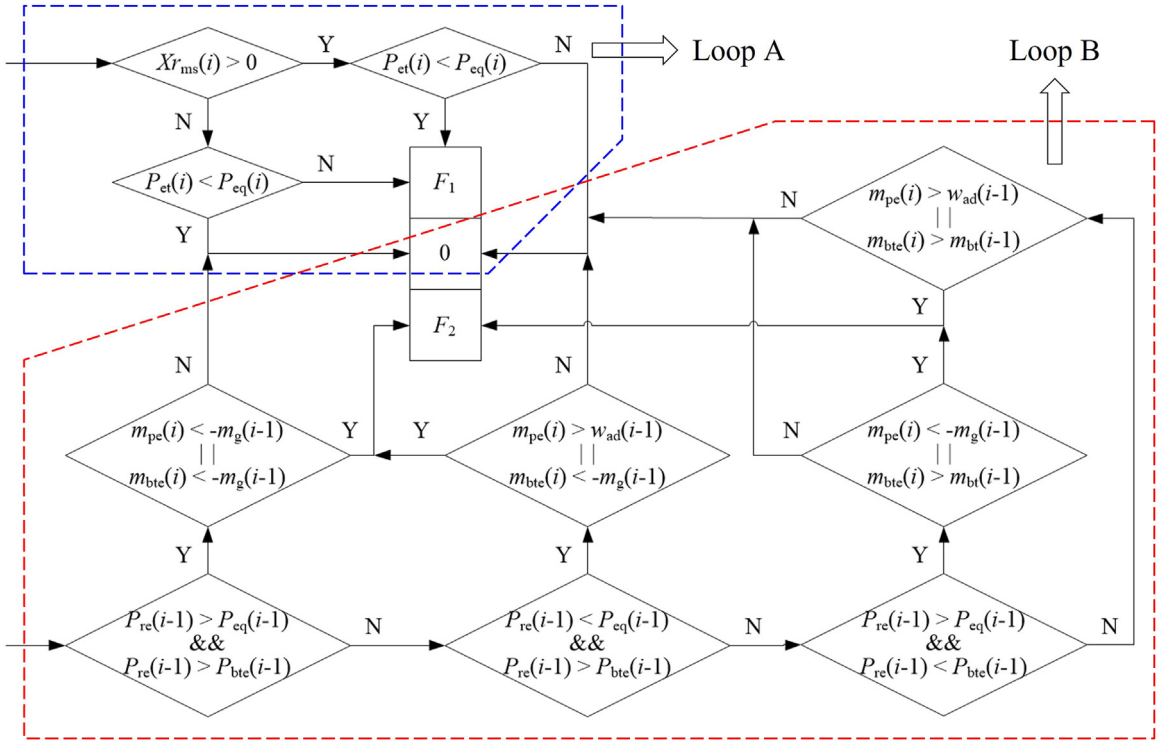

Fig. 9. Logical procedure for the artificial criteria.

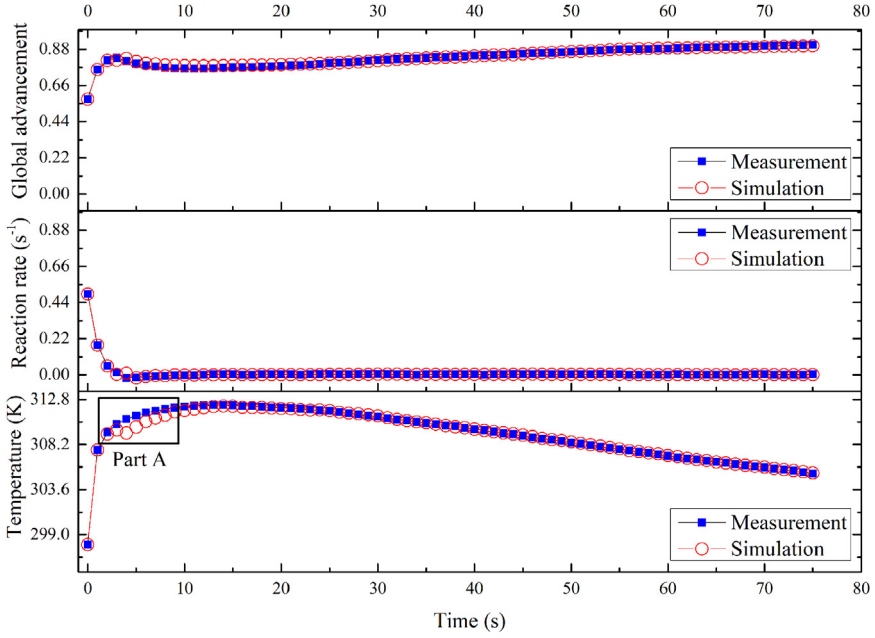

Fig. 10. Fitting results of modeling identification.

and reactor for the simulation were calculated by REFPROP [30], and the coding of the optimization framework was compiled in the MATLAB environment.

The results of the identification and quantification are provided in Fig. 10 and Table 5, respectively. Good consistency between the test and simulation results was obtained. The coefficients of determination when fitting the global advancement, reaction rate, and temperature of the reactor were 0.989, 0.996, and 0.989, respectively. In relation to the mass kinetics, the alternating processes of gas uptake and release were followed accurately. On the other hand, a relatively large deviation in the temperature simulation can be observed in Part A of Fig. 10. This was mainly attributed to the thermal inertia of the system: the reactor was continuously heated during the desorption process by the thermal energy discharged by the previous adsorption processes. The coefficients listed in Table 5 represent the equivalent characteristics of the system, which were difficult to measure. These validate the ability of the proposed framework to determine unrevealed key parameters associated with materials and systems.

Table 4
Parameters of the thermal effects (gas input ≥ 3.42 g).

Number	Parameters	Value
1	c_1	-2.27×10^{-4}
2	c_2	6.53×10^{-3}
3	c_3	-3.15×10^{-2}
4	c_4	5.72×10^{-1}
5	c_5	−23.09
6	c_6	−20.77
7	c_7	−7.47
8	c_8	8.78
9	c_9	0.44
10	c_{10}	1.28×10^{-4}
11	c_{11}	4.72×10^{-3}
12	c_{12}	-2.95×10^{-2}
13	c_{13}	2.03
14	c_{14}	168.25

Table 5
Quantification of the modeling coefficients.

Number	Coefficient	Search range	Value
1	M	0–5	0.39
2	N	0–5	0.18
3	Ar_{ad} (s^{-1})	0–3	1.97
4	Ar_{de} (s^{-1})	0–3	2.94
5	E_{ad} ($kJ{\cdot}mol^{-1}$)	1–3	2.39
6	E_{de} ($kJ{\cdot}mol^{-1}$)	1–3	1.56
7	j_1	–1–0	–0.95
8	j_2	–1–2	–0.14
9	j_3	0–1	0.17
10	j_4	–3–1	–2.18
11	k_1	–1–0	–0.14
12	k_2	–1–5	3.47
13	k_3	0–2	1.11
14	k_4	–2–1	–0.61
15	h ($kW{\cdot}m^{-2}{\cdot}K^{-1}$)	0–1	0.024
16	C_{ad} ($kJ{\cdot}kg^{-13}K^{-1}$)	0–10	2.116

6. Conclusions

This paper proposed an intelligent optimization framework to identify the nonlinear dynamic behavior of a solid-gas sorption system. A lab-scale test rig using activated carbon and carbon dioxide as a working pair was established, and experiments were carried out to investigate the thermal effects of the reaction and dynamic characteristics during the system operation. The changes in the enthalpy and entropy during the physical sorption under different gas mass inputs and uptakes were studied and modeled. In addition, adsorption and desorption tests were conducted to analyze how changes in the gaseous environment influenced the reaction processes. Based on the test results, a dynamic model of the solid-gas sorption system was developed in relation to the global advancement, reaction rate, and reactor temperature. The dynamic factors that influenced the system performance were fully considered in the modeling to facilitate its utilization to solve real engineering problems. To provide an effective method for identifying the modeling coefficients, an optimization framework based on an MGA was developed. Additionally, artificial criteria for tracking the alternating gas uptake and release accompanying the system operation and assisting in the evaluation of the equivalent adsorbate acting during the reaction were integrated into the framework. This further enhanced the optimization ability of the platform, and the identified coefficients were guaranteed to fall within reasonable physical ranges.

To validate the effectiveness of the proposed framework, the simulation results were fitted against the experimental data. The calibration results showed that the proposed modeling could reflect the real performance of the solid-gas sorption process under a changing gaseous environment. On the other hand, the developed intelligent platform could efficiently identify modeling coefficients with a low computation cost (only a small population number and individual number were required). The alternating adsorption and desorption caused by the variation of the thermal effect and changes in the pressure and temperature of the reactor were accurately tracked. Taking the 40 bar case as an example, good agreement of the calibration work was achieved. The coefficients of determination of the modeling replication were 0.989, 0.996, and 0.989 for the global advancement, reaction rate, and temperature, respectively. The population number and corresponding individual number of the MGA were 10 and 20, respectively. The time required to obtain results was less than 3 min (PC: CPU 2.00 GHz, RAM 16 GB), which is acceptable for a real-time identification platform for system operation. Furthermore, the identification results verified that the proposed framework could be utilized as a tool to quantify the unrevealed key parameters related to the material characteristics. For example, the specific capacity heat of the adsorption phase was quantified as $C_{ad} = 2.116$ $kJ{\cdot}kg^{-1}{\cdot}K^{-1}$, which could be used to characterize the degree of physical sorption by comparing the heat capacity of the single solid adsorbent (0.84 $kJ{\cdot}kg^{-1}{\cdot}K^{-1}$) or gas adsorbate (0.849 $kJ{\cdot}kg^{-1}{\cdot}K^{-1}$).

Overall, this study provided an effective dynamic modeling framework for the optimal design and operation of solid-gas sorption systems to help improve energy efficiency and reduce design and operation costs. The proposed intelligent identification method could also contribute to uncovering the key characteristics and operation law of solid-gas sorption at the microscopic level, leading to innovation in the selection of the materials and design of a reactor.

7. Prospective

Based on the current state of research progress, future studies aimed at the further improvement and application of the dynamic modeling framework for solid-gas sorption are summarized as follows.

(1) The gas discharge from the reactor through the open outlet needs to be integrated into the desorption modeling to demonstrate the system performance in real-world application scenarios. Furthermore, thermal inertia needs to be considered in the temperature modeling to increase the fitting accuracy.
(2) With the improvement of the modeling maturity and accuracy, the thermal effects under conditions with low gas inputs (e.g., <3.42 g in Table 3) need to be identified to reveal the filling structure of the adsorbent particles and the gas passages formed inside the reactor.
(3) The system behaviors under different gas input scenarios need to be identified simultaneously to obtain a set of equivalent coefficients that can represent the overall characteristics of the system. Then, the system performance under an intermittent energy input and a fluctuating energy output can be predicted to assist in developing an optimal design plan and control strategy for the system.

Declaration of competing interest

The authors declare that there are no conflicts of interest.

CRediT authorship contribution statement

Dacheng Li: Conceptualization, Methodology, Software, Validation, Writing – original draft, Writing – review & editing. **Tiejun Lu:** Data curation, Investigation, Writing – review & editing. **Nan Hua:** Data curation, Formal analysis, Writing – review & editing. **Yi Wang:** Data curation. **Lifang Zheng:** Supervision. **Yi Jin:** Investigation. **Yulong Ding:** Supervision, Resources. **Yongliang Li:** Funding acquisition, Writing – review & editing, Project administration, Resources.

Acknowledgments

This project received funding from the European Union's Horizon 2020 research and innovation program under Marie Sklodowska-Curie

(Grant No.: 101007976). The authors also express their sincere gratitude to the Engineering and Physical Sciences Research Council (EPSRC) for the funding provided to this project (Grant Nos.: EP/V041665/1 and EP/T022701/1). This work was also financially supported by the National Key Research and Development Program of China (Grant No.: 2021YFE0112500). Additionally, the authors appreciate the support from PCSR at the University of Warwick in the program design and are grateful to Dr. Waseem Aftab from the University of Birmingham for providing SEM test results.

References

[1] T. Li, R. Wang, H. Li, Progress in the development of solid–gas sorption refrigeration thermodynamic cycle driven by low-grade thermal energy, Prog. Energy Combust. Sci. 40 (2014) 1–58.
[2] V. Palomba, S. Nowak, B. Dawoud, et al., Dynamic modelling of Adsorption systems: a comprehensive calibrateddataset for heat pump and storage applications, J. Energy Storage 33 (2021) 102148.
[3] G. Li, S. Qian, H. Lee, et al., Experimental investigation of energy and exergy performance of short term adsorption heat storage for residential application, Energy 65 (2014) 675–691.
[4] Z. Ma, H. Bao, A.P. Roskilly, et al., Seasonal solar thermal energy storage using thermochemical sorption in domestic dwellings in the UK, Energy 166 (2019) 213–222.
[5] P. Gao, X. Wei, L. Wang, et al., Compression-assisted decomposition thermochemical sorption energy storage system for deep engine exhaust waste heat recovery, Energy 244 (2022) 123215 Part B.
[6] G. An, L. Wang, J. Gao, et al., A review on the solid sorption mechanism and kinetic models of metal halide-ammonia working pairs, Renew. Sustain. Energy Rev. 91 (2018) 783–792.
[7] A.A. ElBahloul, E.B. Zeidan, I.I. El-Sharkawy, et al., Recent advances in multistage sorption thermal energy storage systems, J. Energy Storage 45 (2022) 103683.
[8] T. Yan, C. Wang, D. Li, Performance analysis of a solid-gas thermochemical composite sorption system for thermal energy storage and energy upgrade, Appl. Therm. Eng. 150 (2019) 512–521.
[9] F. Xiao, X. Meng, L. Li, et al., Thermos-solid-gas coupling dynamic model and numerical simulation of coal containing gas, Geofluids 2020 (2020) 8837425.
[10] J. Gao, L. Wang, P. Gao, et al., Design and analysis of a gas heating/cooling sorption refrigeration system with multi-salt solid sorbent of $CaCl_2$ and $MnCl_2$, Int. J. Heat Mass Transf. 126 (2018) 39–47.
[11] K.B. Minko, V.I. Artemov, G.G. Yan'kov, Numerical simulation of sorption/desorption processes in metal-hydride systems for hydrogen storage and purification. Part I: development of a mathematical model, Int. J. Heat Mass Transf. 68 (2014) 683–692.
[12] A.A. ElBahloul, E.B. Zeidan, I.I. El-Sharkawy, et al., Experimental and numerical investigation of multistage sorption energy storage system, Appl. Therm. Eng. 218 (2023) 119313.
[13] T. Ajzoul, C. Chaussavoine, M. Amouroux, Finite element analysis of a transient nonlinear heat transfer problem, Comput. Chem. Eng. 19 (1995) 423–436.
[14] M. Mbaye, Z. Aidoun, V. Valkov, et al., Analysis of chemical heat pumps (CHPs): basic concepts and numerical model description, Appl. Therm. Eng. 18 (1998) 131–146.
[15] V.F.D. Martins, C.V. Miguel, J.C. Gonçalves, et al., Modeling of a cyclic sorption–desorption unit for continuous high temperature CO_2 capture from flue gas, J. Chem. Eng. 434 (2022) 134704.
[16] M. Lebrun, B. Spinner, Models of heat and mass transfers in solid–gas reactors used as chemical heat pumps, Chem. Eng. Sci. 45 (1990) 1743–1753.
[17] N. Mazet, M. Amouroux, B. Spinner, Analysis and experimental study of the transformation of a non-isothermal solid/gas reacting medium, Chem. Eng. Commun. 99 (1991) 155–174.
[18] N. Mazet, M. Amouroux, Analysis of heat transfer in a non-isothermal solid-gas reacting medium, Chem. Eng. Commun. 99 (1991) 175–200.
[19] H. Huang, G. Wu, J. Yang, et al., Modeling of gas–solid chemisorption in chemical heat pumps, Sep. Purif. Technol. 34 (2004) 191–200.
[20] R.K. Nagamalleswara, M. Ramgopal, S. Bhattacharyya, Development of thermodynamic and reaction kinetic data on $BaCl_2$-NH_3 system with and without expanded natural graphite, Sci. Technol. Built Environ. 23 (2017) 1203–1211.
[21] H. Bao, Y. Wang, A.P. Roskilly, Modelling of a chemisorption refrigeration and power cogeneration system, Appl. Energy 119 (2014) 351–362.
[22] O.F. Cruz, I.C. Gómez, F. Rodríguez-Reinoso, et al., Activated carbons with high micropore volume obtained from polyurethane foams for enhanced CO_2 adsorption, Chem. Eng. Sci. 273 (2023) 118671.
[23] T.H. Rupam, Md.A. Islam, A. Pal, et al., Thermodynamic property surfaces for various adsorbent/adsorbate pairs for cooling applications, Int. J. Heat Mass Transf. 144 (2019) 118579.
[24] S.O. Akpasi, Y.M. Isa, Effect of operating variables on CO_2 adsorption capacity of activated carbon, kaolinite, and activated carbon – kaolinite composite adsorbent, Water Energy Nexus 5 (2022) 21–28.
[25] J. Serafin, B. Dziejarski, Application of isotherms models and error functions in activated carbon CO_2 sorption processes, Microporous Mesoporous Mater. 354 (2023) 112513.
[26] P. Neveu, J. Castaing-Lasvignottes, Development of a numerical sizing tool for a solid-gas thermochemical transformer—I. Impact of the microscopic process on the dynamic behaviour of a solid-gas reactor, Appl. Therm. Eng. 17 (1997) 501–518.
[27] M.T. Howerton, Thermochemical energy storage system and heat pumps. Martin Marietta Aerospace, Report SAE/P78/75. (1978) 935–940.
[28] X. Shi, W. Long, Y. Li, et al., Research on the performance of multi-population genetic algorithms with different complex network structures, Soft Comput. 24 (2020) 13441–13459.
[29] S.H. Zegordi, M.A.B. Nia, A multi-population genetic algorithm for transportation scheduling, Transp. Res. E 45 (2009) 946–959.
[30] E.W. Lemmon, I.H. Bell, M.L. Huber et al., NIST Standard Reference Database 23: reference fluid thermodynamic and transport properties-REFPROP, Version 10.0, National Institute of Standards and Technology, Standard Reference Data Program. Gaithersburg. (2018)